Acta Mech 227, 2577–2594 (2016)
DOI 10.1007/s00707-016-1633-2

ORIGINAL PAPER

**C. Sri Harsha · C. S. Prasanth · B. Pratiher**

# Prediction of pull-in phenomena and structural stability analysis of an electrostatically actuated microswitch

Received: 9 October 2015 / Revised: 25 March 2016 / Published online: 17 May 2016


**Abstract** The present study is concerned with the theoretical investigation of pull-in phenomena and their significance for assessing structural instability of a MEMS switch, modeled as electrostatically actuated micro-cantilever beam coupled with a rigid plate. The essential factors such as geometric and inertial nonlinearities, higher-order distribution of electrostatic pressure, and nonlinear squeeze film effect have been included in the dynamic model to accurately predict the pull-in voltages. The limit of structural stability due to pull-in behavior is numerically illustrated for both static and dynamic conditions of the device. The effects of varying the electrode length, structural nonlinearity, air-gap thickness, and plate length on pull-in instability are investigated. The pull-in voltage predicted numerically within the limit of operational voltage has been validated with the findings in 3D modeling software. It is perceived that a highly deformable micro-system loses its stability at high actuation voltage via static bifurcation due to pull-in instability. Furthermore, structural stability appears observed to be high by reducing the size of the device as the pull-in occurrence is at high applied voltage. The damping mechanism introduced into the device essentially stabilizes the device by switching the pull-in voltage to a high value. However, the obtained outcomes enable the satisfactory predictions of pull-in occurrence and subsequent understanding of structural instability and safe operating zones of the device.

## 1 Introduction

Nowadays, the use of electrostatically actuated micro-/nano-electromechanical systems has satisfactorily been adopted for designing and developing various MEMS devices such as microswitches, micro-motors, micro-relays, micro-grippers, micro-resonators, micro-mirrors, micro-pumps, micro-valves, and micro-filters [1]. Due to simplicity in design with low-cost fabrication, fast response, the ability to achieve rotary motion, and low power consumption, the utilization of electrostatic actuation in MEMS applications has tremendously escalated [2]. However, this actuation gives rise to a complex nonlinear phenomenon and often results in the structural instability via bifurcation due to pull-in occurrence for the finite air-gap thickness of the order of $10^{-5}$ or higher. As the pull-in behavior restricts the stable travel range, evaluating the pull-in voltage plays a decisive and inevitable factor in understanding the stable operation zones and revealing the causes of structural

C. Sri Harsha · C. S. Prasanth · B. Pratiher (✉)
Mechanical Engineering, Indian Institute of Technology, Jodhpur 342011, India
E-mail: barun@iitj.ac.in

failure. However, the performance of electrostatically actuated MEMS devices is limited due to the existing inherent pull-in instability. Here, the microswitch has been modeled as micro-cantilever beam coupled with a rigid plate under electrostatic actuation. The present model comprises unique and distinct features with compendious outcomes that contrive the clear portrait of possible existing pull-in instability when the design parameters vary within a certain range.

However, in this Subsection, a brief state of the art of the research on electrostatically actuated MEMS devices has been discussed. Adams et al. [3] showed the behavior of a micromechanical device when the linear and nonlinear stiffness coefficients are tuned independently. Kim et al. [4] studied the mechanical behavior of a micro-cantilever based on the intrinsic strain during deposition of MEMS structures. Shenthilkumar et al. [5] dealt with pull-in instability of electrostatically actuated beams having the configurations of cantilever beam, fixed–fixed beam and modified beam structures with perforations of square, rectangular and circular shapes using COMSOL 4.3 software. Lee et al. [6] analyzed nonlinear dynamic responses of a micro-cantilever for atomic force microscopy numerically as well as experimentally. The frequency response function of an initially excited micro-cantilever on a squeeze film was developed by Lee [7] using the mode superposition method. In [8,9], vibration characteristics of a moving part, the switching speed and long-term reliability of MEMS switch have been investigated, and the effect of maximum toggle rate of MEMS due to the resonant frequencies of a micro-cantilever has been reported. Several methods have been used to calculate the pull-in stability of electrostatically actuated MEMS devices as the operational range of electrostatic devices is usually limited [10–12]. Dynamic pull-in voltage and behavior are necessitated and are a significant factor in operating the electrostatically MEMS devices beyond the actuation voltage, i.e., voltages exceeding the pull-in [13]. Abdel-Rahman et al. [14] investigated the effect of geometric nonlinearity on the pull-in conditions, while Haluzan et al. [15] controlled the pull-in voltage by adjusting the gap shape in an electrostatically actuated cantilever and fixed–fixed beams. Dominicus et al. [16] developed a single-element approach for the electrostatic actuation, and they modeled an air-gap capacitor as lumped spring–mass system to determine its behavior. Mojahedi et al. [17] studied the nonlinear vibrations of multilayer micro-plates subjected to the electric field. Some of the researchers as Busta et al. [18] introduced a conductive shield with an opening between the movable MEMS component and substrate to control pull-in forces and to increase pull-in voltages. Zhang and Meng [19] simulated the resonant amplitude frequency responses of an electrostatically actuated micro-cantilever under combined parametric and forced excitations using the harmonic balance method. Similar research has also been carried out by Liu et al. [20] using Poincaré mapping to characterize the nonlinear dynamic behavior and to find the region of bi-stability for the closed loop at low gain. Li and Aluru [21] proposed meshless techniques for effective simulation of linear and nonlinear behavior in electrostatic MEMS. Ashby [22] suggested an approach to select materials for the design of macroscale structures. Gabbay et al. [23] developed reduced-order dynamic macro-models of MEMS devices to capture the device behavior for rapid circuit and system simulation. Furlani [24] investigated the effects of nonlinearity on the behavior of parametric resonance of a micro-machined oscillator. They have also shown analytically how the nonlinearity changes the stability characteristics of parametric resonance significantly. Krylov and Mainom [25] studied the nonlinear behaviors near the pull-in voltage of an electrically actuated micron-scale beam using the Galerkin procedure. Chao et al. [26] investigated the precise predictions of the DC dynamic pull-in voltages of a clamped–clamped microbeam based on a distributed model. A step function of voltage has been considered to introduce the DC dynamics for analyzing the pull-in phenomenon. Chatterjee and Pohit [27] formulated a comprehensive model of an electrostatically actuated micro-cantilever beam separated from the ground plane by a relatively larger gap accounting for the nonlinearities of the system arising out of electric forces, geometry of the deflected beam, and the inertial terms. The higher-order correction of electrostatic forces has been incorporated into the dynamic model for analyzing the pull-in phenomenon. Pratiher [28] demonstrated the stability and bifurcation analysis of a highly nonlinear electrically driven MEMS resonator derived by using Hamilton's principle and Galerkin's method considering both transverse and longitudinal displacement of the resonator. Kivi et al. [29] investigated both static and dynamic behaviors of a fully clamped functionally graded piezoelectric microbeam when it is subjected to simultaneous electrostatic and piezoelectric actuations. Authors have shown that tunability of the bending stiffness due to piezoelectric actuation can be used to stabilize the system from the pull-in instability. Moreover, the effect of surface traction as described by Casimir force or van der Waals force due to molecular interaction between two surfaces plays an important role in determining the pull-in deflection in microswitches depending on the gap between the electrodes [30,31]. Moeenfard et. al [32] investigated the effect of van der Waals force on the calculation of pull-in voltage of an electrostatically coupled two-degree-of-freedom model which considers both bending and torsion of the supporting torsion beams. They showed that for relatively low stiffness ratio, i.e., ratio of bending stiffness to the torsion stiffness, the bending moment is considered to be

the dominant instability mode. Ramezani and Alasty [33] studied the pull-in voltage of cantilever arrays with the combined electrostatic and Casmir or Van der Waals interactions between the neighboring beams. Wang et al. [34] determined the deflection of microfabricated rectangular membrane strips driven electrostatically with the attractive Casimir force between the conducting surfaces under consideration. It has been shown in the paper that the influence of Casimir forces on the deflection is dependent on the values of the initial gap between the structures. Recently, Duan et al. [35] investigated the pull-in instability of a cantilever nano-actuator model incorporating the effects of the surface, the fringing field, and the Casimir attraction force by selecting a quartic polynomial as the shape function of the beam obtained by satisfying all of the four boundary values.

Regardless of other aspects of MEMS modeling, the effect of the squeeze film is inevitable for accurately estimating the dynamic performance of MEMS devices, and its availability in the dynamic model accomplishes meticulous outcomes for designing such devices [25,36,37]. McCarthy et al. [38] considered the effect of a squeeze film for obtaining the transient behavior near the critical voltage of two different electrostatically actuated microswitch configurations using finite difference analysis. Rocha [39] proposed a novel technique for measuring the damping constant at different gap sizes that lead to the further improvement in accuracy of the squeeze film models. Veijola [40] developed a compact model in evaluating the dynamic characteristics of the device considering the effect of the squeeze film.

Nonetheless, a number of researchers were investigating the pull-in instability under electrostatic actuation for the MEMS devices models based on either Euler–Bernoulli beam with small deformation theory or combination of discrete spring–mass–damper components. It has also been glimpsed that almost all the researchers have considered parallel approximation theory even after accounting for geometric nonlinearity due to mid-pane stretching in their mathematical models. A limited number of researchers have considered geometric as well as inertial nonlinearities in their respective mathematical models for calculating the pull-in voltage. However, the geometric nonlinearity may introduce a higher-order electrostatic force and can be an inevitable factor in computing the pull-in behavior when the microsystem undergoes large elastic deformation [27,28]. While AC potential difference has been considered in [28], a bias DC voltage has been chosen in [27] for investigating the pull-in phenomena. In both of these works, the effect of squeeze film damping was not considered, which cannot be ignored for the microsystem with a smaller air-gap thickness. In addition, squeeze film damping is unavoidable when the microsystem undergoes large motions. Considering air damping in the dynamic model and its effect on dynamic pull-in have been studied in [25,36–40]. The effect of AC potential on the characteristics of the pull-in phenomenon has been studied in [13]. It has been obtained that a new switch uses a voltage much lower than the traditionally used DC voltage.

The dynamic model neglecting the nonlinearities arising strongly due to mid-plane starching was developed under the frame of parallel plate approximation for constructing the electrostatic force in most of existing research works. However, the development of small-size MEMS devices often leads to a moderately large gap ratio typically of the order of $10^{-3}$ or even higher. For such conditions, the parallel approximation theory is improper in calculating the pull-in voltage since the nonlinear higher-order electrostatic force exists for a larger air gap between the electrodes. In addition, the structural nonlinearity must be accounted for when the deformable electrode undergoes large elastic deformation. This type of nonlinearity furnishes both geometric and inertial nonlinearities and must be considered in the mathematical model. While geometric nonlinearity controls the static pull-in voltage, both geometric and inertial nonlinearities influence dynamic pull-in voltage. However, in [27,28] the effect of these nonlinearities on pull-in characteristics for cantilevered-based microsystems has been investigated without considering the squeeze film damping and a rigid plate attached at the end.

In the present work, an attempt has been made to illustrate the pull-in voltage and its negative influences on structural stability of a microbeam coupled with rigid plate-based microswitch under the disparity of several design parameters. This configuration is fruitful and worthwhile while designing the microsystem which works to alternate ON and OFF conditions across the bias pull-in voltage. Here, most of the important features to develop an accurate MEMS device have been introduced which remained unexplored by the researchers earlier. Here, the geometric and inertial nonlinearities have been included along with nonlinear squeeze film damping to originate an error-free model, which was not developed earlier. Hence, the pull-in voltage and its liability on structural instability via bifurcation have been investigated for a microswitch modeled as a micro-cantilever beam coupled with a rigid plate actuated electrostatically. In the mathematical model, higher-order electrostatic pressure, geometric and inertial nonlinearities, and nonlinear squeeze film damping along with linear viscous damping have been considered. The authors are here striving earnestly to appropriately reestablish the objectives articulated earlier in [25] for investigating the pull-in behaviors. Here, a micro-cantilever coupled with a rigid

plate at the end subjected to electrostatic actuation has been preferred as compared to the works [27,28]. The couple of microbeam with rigid plate may effectively reduce the dynamic pull-in voltage so that the microswitch can efficiently run at a relatively small applied voltage. Further, the effect of squeeze film damping has been incorporated in contrast to the developments [27,28]. Hence, the results obtained in this work are absolutely different from the results obtained in previously published works [25–28]. The loss of stability due to pull-in has been exhaustively portrayed, and an in-depth analysis of pull-in occurrences has been given.

## 2 Mathematical approximation

A schematic diagram of a cmicroswitch is characterized by a micro-cantilever coupled with a rigid micro-plate subjected to higher-order distribution of electrostatic pressure as shown in Fig. 1. The concept of the Euler–Bernoulli theorem has been adopted for deriving the equation of motion that governs the dynamic characteristics and its pull-in behavior under a bias DC potential. The electrostatic force has been assumed to be uniform across the width and small strain of the microbeam under the statutory of large deformation via the consideration of nonlinear curvature. Transverse $v(x,t)$ and axial $u(x,t)$ displacement components occur along the inertial directions ($z$,$x$) of the beam centroid axis under the potential difference. The relation between the variables $v(x,t)$ and $u(x,t)$ is constituted by a constraint equation $\left(1+u'\right)^2+v'^2=1$ of the beam known as an inextensibility condition. Hence, the longitudinal displacement $u(x,t)$ can explicitly be written as $u\left(\xi,t\right)=\int_0^{\xi}\sqrt{1-v'^2}\mathrm{d}x-\xi$ in terms of the transverse deflection $v(x,t)$. However, the total kinetic energy of the structure consisting of the microbeam and rigid plate is expressed as

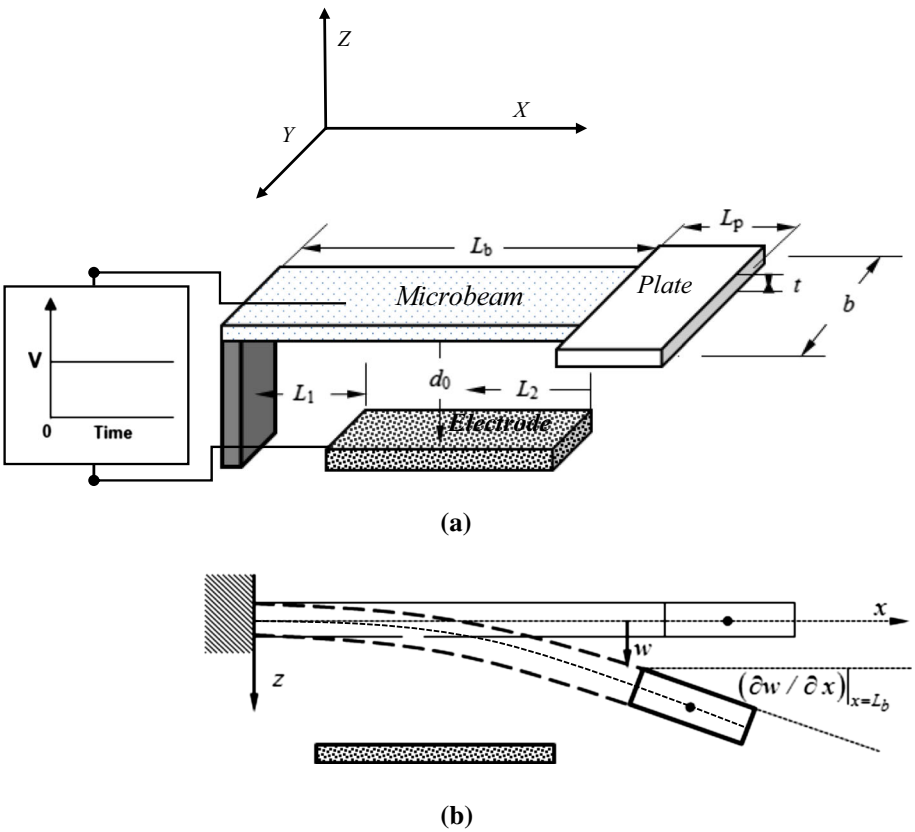


**Fig. 1** Graphical representation of a cantilever-based microstructure coupled with a rigid plate

$$K = \frac{1}{2}\int_0^{L_b} \rho A\left(\dot{v}^2 + \dot{u}^2\right) \mathrm{d}x + \frac{1}{2}\int_0^{L_b} M\left(\dot{v}^2 + \dot{u}^2\right)\delta\left(x - L_b\right) \mathrm{d}x + \frac{ML_p}{2}\int_0^{L_b} \left\{\frac{\partial}{\partial t}\left(v\right) \cdot \frac{\partial}{\partial t}\left(v'\right)\right\}\delta\left(x - L_b\right) \mathrm{d}x$$
$$+\frac{1}{2}\int_0^{L_b} \left(J + ML_p^2\right)\left\{\frac{\partial}{\partial t}\left(v'\right)\right\}^2 \delta\left(x - L_b\right) \mathrm{d}x. \tag{1}$$

Prime $()'$ and $()^{\bullet}$ are denoting the differential with respect to space and time. Here, $M$, $l_c$, $\rho$, $A$, $L_b$, and $J$ are mass of rigid plate, distance from the beam end to centroid of rigid plate, mass density of the beam element, cross-sectional area of the beam element, length of the beam and rotational moment of the rigid plate around the beam end, respectively.

By the definition of slope, $\sin\phi = v'$, radius of nonlinear curvature $(k) = \frac{\partial\phi}{\partial x} = \phi'$ and corresponding bending moment $M\left(x\right) = EIv''/\left(\sqrt{1 - v'^2}\right)$, the potential energy due to large elastic deformation stored in the microbeam element has been expressed since the potential energy of the rigid body is negligible as

$$V = \int_0^{L_b} EI \cdot k^2 \mathrm{d}x = \int_0^{L_b} EI \cdot \left(v''^2 + v''v'^2\right)\mathrm{d}x. \tag{2}$$

Here, $E$ and $I$ are Young's modulus and area moment of inertia, respectively. The potential energy generated due to electrostatic actuation between the microbeam and grounded plate has been expressed [25] neglecting the fringing effect,

$$V_e = \frac{\varepsilon_0 bV^2}{2}\int_0^{L_b} \frac{1}{\left(d_0 - v\right)}\left\{1 + \frac{1}{3L_b^2}\left(d - v\right)'^2\right\} H\left(x - L_1\right) H\left(x - L_2\right) \mathrm{d}x. \tag{3}$$

Here, the permittivity of the vacuum $\varepsilon_0$ is equal to $8.856 \times 10^{-1}\mathrm{C}^2\mathrm{N}^{-1}\mathrm{m}^{-2}$. Also, $b$, $V$, $L_1$, and $L_2$ are width of the microbeam, applied voltage, mass of rigid plate, location of the starting point and ending point of the electrode from the fixed end, respectively. A stepwise function $H\left(x\right)$ has been used to denote the area-wise effect of electrostatic pressure. The work done by the non-conservative damping force due to the squeeze film effect for $\left(d_0 - v\right) \ll L_b$ has been expressed as

$$\delta W_{nc} = -\int_0^{L_b} F_s \frac{\partial}{\partial t}\left(d - v\right)\delta v + HOF. \tag{4}$$

Here, $F_s = \mu\frac{b^3}{\left(d_0 - v\right)^3}$. Also, $\mu$ is the effective viscosity of the fluid flow in the air gap [36]. Using extended Hamilton's principle $\int_{t_1}^{t_2}\left(\delta K - \delta V + \delta W_{nc}\right)\mathrm{d}t = 0$, $\delta v\left(t_1\right) = \delta v\left(t_2\right) = 0$, and procedures similar to the works [27,28] and eliminating the higher-order squeeze film damping effect, one may obtain the following differential equation of motion in terms of transverse deflection $v$:

$$\rho A\frac{\partial^2 v}{\partial t^2} + c\dot{v} + EI\left[v'''' + \left\{v'\left(v'v''\right)'\right\}'\right] + \rho A\left[v'\int_L^{\eta}\int_0^{\xi}\left(\ddot{v}v' + \dot{v}'^2\right)d\eta d\xi\right]' + \frac{\mu b^3}{\left(d_0 - v\right)^3}\frac{\partial}{\partial t}\left(d_0 - v\right)$$
$$= \frac{\varepsilon_0 bV^2}{2\left(d_0 - v\right)^2}\left[1 - \frac{1}{L_b^3}\left\{v'^2 + 2\left(d_0 - v\right)v''\right\}\right]\left\{H\left(x - L_1\right) H\left(x - L_2\right)\right\} \tag{5}$$

With associated boundary conditions:

$$\begin{aligned}
&\text{at } x = 0: \quad v\left(0,t\right) = 0,\ v'\left(0,t\right) = 0;\\
&\text{at } x = L: \quad EIv'''\left(L,t\right) = M\ddot{v}\left(L,t\right) + Ml_c\ddot{v}'\left(L,t\right),\\
&\qquad EIv''\left(L,t\right) = -l_c M\ddot{v}\left(L,t\right) + 4Ml_c^2\ddot{v}'/3\left(L,t\right).
\end{aligned} \tag{6}$$

The inertia force and moment due to the presence of a rigid plate at the end act at the end of the beam and appear in the boundary condition at $x = L$. Substituting the non-dimensional parameters: $s = (x/L_b)$, $\tau = t\left(EI/\rho AL_b^4\right)^{1/2}$, $w = (v/d_0)$, $\beta = (d_0/L_b)^2$, $\overline{L}_1 = (L_1/L)$, $\overline{M} = (M/\rho AL_b)$, $\alpha = \left(6\varepsilon_0 L_b^4/Eh^3d_0^3\right)^{1/2}$, $\overline{c} = c(L_b^4/EI\rho A)^{1/2}$, $\overline{\mu} = \mu(b/d_b)(\rho AL_b^4/EI)^{1/2}$, $\overline{L}_2 = (L_2/L_b)$, and $\overline{L}_c = (l_c/L_b)$ into Eq. (5), one can rewrite the equation of motion (5) into the non-dimensional form of equation of motion as follows:

$$\rho A\frac{\partial^2 w}{\partial t^2} + \overline{c}\dot{w} + EI\left[w'''' + \beta\left\{w'\left(w'w''\right)'\right\}'\right] + \beta\left[w'\int_1^{\overline{\eta}}\int_0^{\overline{\xi}}\left(\ddot{w}w' + \dot{w}'^2\right)d\overline{\eta}d\overline{\xi}\right]' + \frac{\overline{\mu}b^3}{(1-w)^3}\frac{\partial}{\partial\tau}(1-w)$$
$$= \frac{\alpha}{(1-w)^2}\left[1 - \frac{\beta}{3}\left\{w'^2 + 2(1-w)w''\right\}\right]\left\{H\left(s-\overline{L}_1\right)H\left(s-\overline{L}_2\right)\right\}, \tag{7}$$

$$\rho A\frac{\partial^2 w}{\partial t^2} + \overline{c}\dot{w} + EI\left[w'''' + \beta\{\text{ geometric nonl.}\}\right] + \beta[\text{inertial nonl.}] + \text{Non. Sq. Damping}$$
$$= \frac{\alpha}{(1-w)^2}\left[1 - \frac{\beta}{3}\{\text{HOD Elect. Pressr.}\}\right]\left\{H\left(s-\overline{L}_1\right)H\left(s-\overline{L}_2\right)\right\}. \tag{8}$$

The boundary conditions are

$$\text{at } s = 0: \quad w = 0, \ \frac{\partial \mathrm{w}}{\partial \mathrm{s}} = 0,$$
$$\text{at } s = 1: \quad w''' = \overline{M}\frac{\partial^2 w}{\partial\tau^2} + \overline{ML}_c\frac{\partial^3 w}{\partial\tau^2\partial \mathrm{s}}, \ w'' = -\overline{L}_c\overline{M}\frac{\partial^2 w}{\partial\tau^2} - \frac{4}{3}\overline{ML}_c^2\frac{\partial^3 w}{\partial\tau^2\partial \mathrm{s}}. \tag{9}$$

It is observed that the influences of both geometric and inertial nonlinearities onto the pull-in occurrence are strictly by the air-gap thickness ($d$) keeping the length of the beam constant. Furthermore, if $\beta << 1$, the effect of structural nonlinearities is negligible, governed and the system can be brought to a simple linear time invariant system where a parallel plate approximation can satisfactorily be applied to represent the electrostatic pressure distribution. The time-dependent terms have a significant effect on the calculation of dynamic pull-in voltage of the micro-devices, but do not influence the static pull-in behavior. Neglecting the term $\left(\overline{\mu}b^3/(1-w)^3\right)\frac{\partial}{\partial\tau}(1-w)$, the piecewise effect of electrostatic pressure and rigid plate attached at the end, the present equation of motion (7) is similar to that expressed in [27,28]. Similarly, the present equation of motion neglecting the terms of higher-order distribution of electrostatic pressure and nonlinear geometric and inertial terms can also be similar to the equation obtained in [25] assuming parallel plate assumption accounting for small deflection theory. Nonetheless, the outcomes obtained here are distinct and included various facets of MEMS technology to develop an accurate mathematical model with pertinent quality assessment of pull-in instability in electrostatically actuated MEMS devices.

## 3 Generalized decomposition: Galerkin's principle

The motion configuration of the deflection of an electrostatical actuation microsystem can be written as:

$$w(s,\tau) = \sum_{n=1}^{n}\gamma_j(s)\,\mathrm{e}^{i\omega\tau}, \ n = 1,2,3\ldots\infty, \quad 0 \le s \le 1. \tag{10}$$

Here, $\mathrm{e}^{i\omega\tau}$ is the time modulation that results in varying the vibration amplitude with respect to time, and $\gamma_j(s)$ is an admissible function that is obtained by satisfying the boundary conditions, both essential and forced, and not necessarily the equation of motion. A single admissible trial function $\gamma_1(s) = \gamma(s)$ has been used for solving the problem since the first mode is observed to be the dominant mode of the system. However, the following admissible function similar to that of the eigen function of the cantilever beam with heavy tip body has been used to calculate the pull-in behavior:

$$\gamma_n(s) = \{\cosh(\beta_n s) - \cos(\beta_n s)\} + \Gamma_n(\sinh(\beta_n s) - \sin(\beta_n s)). \tag{11}$$

Here,

$$\Gamma_n = \frac{\sin\ \beta_n s\ (1\ -\ \overline{M}\beta_n^2 L)\ -\ \sinh\ \beta_n s\ (1\ -\ \overline{M}\beta_n^2 L)\ +\ \left(\overline{M}\beta_n\right)\{\cos\beta_n s - \cosh\beta_n s\}}{\cos\ \beta_n s\ (1\ -\ \overline{M}\beta_n^2 L)\ -\ \cosh\ \beta_n s\ (1\ +\ \overline{M}\beta_n^2 L)\ +\ \left(\overline{M}\beta_n\right)\{\sin\beta_n s - \sinh\beta_n s\}}.$$

The characteristic value $\beta_n$ can be obtained from the following characteristic equation:

$$1\ +\ \frac{1}{3}\ L^2\overline{M}\beta_n^4\ +\ \cos\beta_n\ \cosh\beta_n\left(1\ -\ \frac{1}{3}\ L^2\overline{M}\beta_n^4\right) +\ \cos\beta_n\ \sinh\beta_n\left(\overline{M}\beta_n\ -\ \frac{4}{3}\ L^2\overline{M}\beta_n^3\right)$$
$$-\cosh\beta_n\ \sin\beta_n\left(\overline{M}\beta_n\ +\ \frac{4}{3}\ L^2\overline{M}\beta_n^3\right)\ -\ 2\frac{4}{3}\ L\overline{M}\beta_n^2\sinh\beta_n\ \sin\beta_n\ =\ 0. \tag{12}$$

The coefficient of the equation has been evaluated by using Galerkin's technique $\int_0^{L_b} R\,(s,t)\,\gamma_n\,(s)\ \mathrm{d}s\ =\ 0$, where $R\,(s,t)$ is the residue operator, and $\gamma_n\,(s)$ is an admissible function of $n$th mode considered to be the same as that of the admissible function (11).

## 4 Results and discussion

The derived equation of motion has been used for analyzing the qualitative and quantitative assessment of structural stability under static and dynamic pull-in behavior which was not thoroughly explored earlier. The effect of electrode length, air-gap thickness, higher-order distribution of electrostatic pressure and structural nonlinearity has been considered for estimating the critical pull-in voltage and realized the limit of applied voltage for both beam and plate ends. Evaluating static pull-in voltage, also called as collapse voltage, is essential to understand the stability losses for steady applied voltage, i.e., the rate of change of voltage is assumed to be negligible, whereas the estimation of dynamic pull-in behavior is an important consideration for $\mathrm{d}V\ \neq\ 0$ in designing an electrostatically actuated microsystem, and it reveals the limitation of applied voltage at which the system loses its stability via dynamic pull-in phenomena. Here, dynamic motion of the device plays a significant role to find out the pull-in voltage. However, a metallic beam with length 300 μm, width 20 μm, thickness 2 μm, and air-gap thickness 2 μm is chosen, while length and width of the rigid plate are chosen as 60 μm, and 38 μm, respectively. The thickness of the plate has been taken the same as that of the beam.

### 4.1 Static analysis

Here, the deflection of the beam end and plate end has been depicted under steady-state voltage directly by solving the boundary value problem (BVP) setting all time derivatives in Eq. (8) equal to zero. Since Eq. (8) includes several nonlinear terms, the system may exhibit multiple approximate solutions, and the solutions are dependent on the initial guess values. However, the only stable solutions are those practically realized by the system. In static analysis, approximate solutions have been obtained for absolute and relative tolerances of the order of $10^{-6}$.

The pull-in voltage has been obtained numerically using MATLAB 8.5 and verified with the findings performed in 3D modeling software where an electrostatically actuated micro-cantilever beam coupled with the plate has been developed and simulated. The entire device was assumed to be made of polysilicon with Young's modulus ($E$) = 169 GPa, Poisson's ratio ($\vartheta$) = 0.223, and air gap = 2 μm and considering the relative permittivity value equal to 1. The microbeam resides in an electrically insulated air-filled chamber, and the lower side of the chamber has been considered as grounded electrode. While the micro-cantilever beam coupled with the plate has been meshed using swept mesh, dividing the length of the beam into 20 elements, the electrodes surface has been meshed using a free Quad type of element with maximum element size = 4 μm and minimum element size = 0.064 μm. Figure 2 depicts the mesh of a cantilever-based microbeam coupled with a rigid plate in 3D modeling software. The obtained non-dimensional results are then converted from the non-dimensional deflection $w$ to the dimensional variable $v$ to compare it with the results obtained using modeling software. As an example, the elastic deformed shape of the switch for a certain applied electrostatic actuation obtained using 3D modeling software has been displayed in Fig. 2b where the red contour represents the maximum

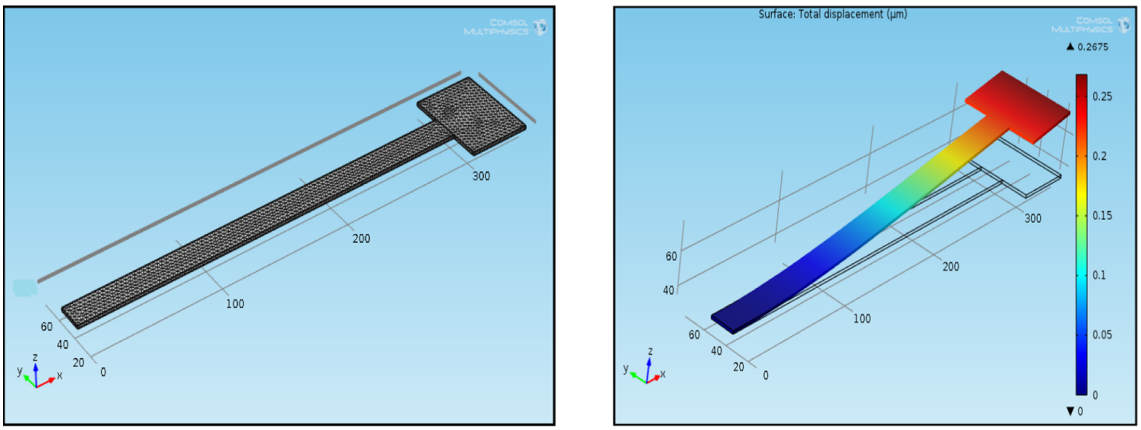


(a) (b)

**Fig. 2** **a** Meshing of cantilever-based microstructure coupled with rigid plate in COMSOL, **b** Deflection of cantilever-based microstructure coupled with rigid plate in COMSOL under electric actuation

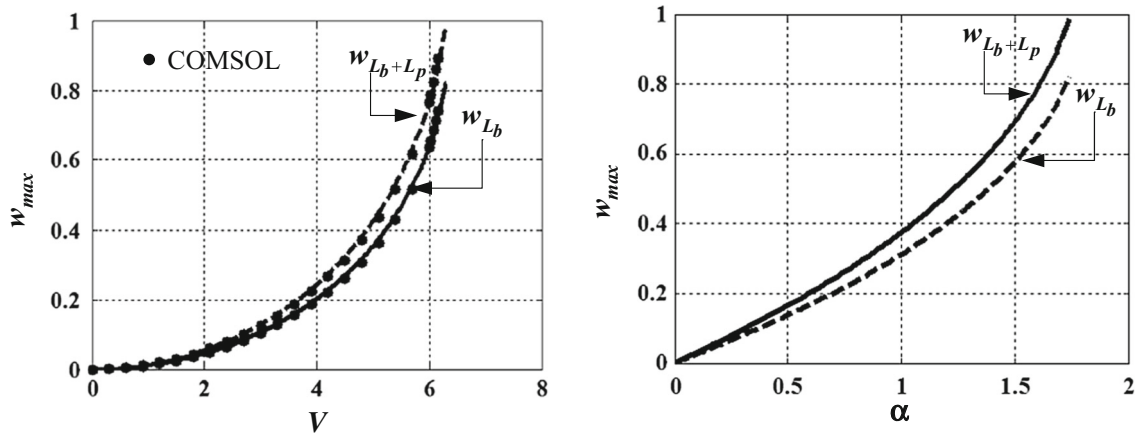


(a) (b)

**Fig. 3** **a** Maximum deflection of beam end ($w_{L_b}$) and plate at end ($w_{L_b+L_p}$) under actuation voltage for $(d_0/L_b)^2 = 4.4\text{e}^{-5}$. **b** Maximum deflection of beam end ($w_{L_b}$) and plate at end ($w_{L_b+L_p}$) under electrostatic pressure for $(d_0/L_b)^2 = 4.4\text{e}^{-5}$

deflection. The deflection at the end points of microbeam and plate for various applied voltages is illustrated in Fig. 3. However, the deflection at the plate end depicts the actual displacement perceived practically by the system. For finding the deflection at plate end $w|_{L_b+L_p}$ ,slope $\frac{\partial w}{\partial s}$ of the microbeam at the end point $L \cdot L_b$ it is sufficient to multiply with the length of rigid plate since slope and geometric curvature built at tip of the beam element remains the same for every point over the plate length shown in Fig. 1b. The effect of geometric nonlinearity due to moderately large elastic deformation on the pull-in behavior has been investigated for applied voltage starting from zero to the critical value. Figure 3 represents the maximum deflections ($w$) at beam end and plate end, respectively, which are precisely computed until the applied voltage reaches to its critical value at which the system becomes statically unstable as the electrostatic force exceeds the restoring force. Since, in most of the communication and power circuits systems, the application of the electrostatically actuated microswitch is largely devoted to alternate ON and OFF conditions by tuning a bias voltage across the pull-in back and forth, it is hence desirable to design and develops an efficient and effective MEMS switch which can operate at low actuation voltage for performing the suitable task.

Figure 4 displays the effect of air-gap thickness ($d$) on the pull-in instability. It has been observed that the electrostatically actuated MEMS switch with small $d$ operates mainly at a low actuation voltage. Steady-state amplitude of motion for every applied voltage has been observed until the applied voltage reaches a

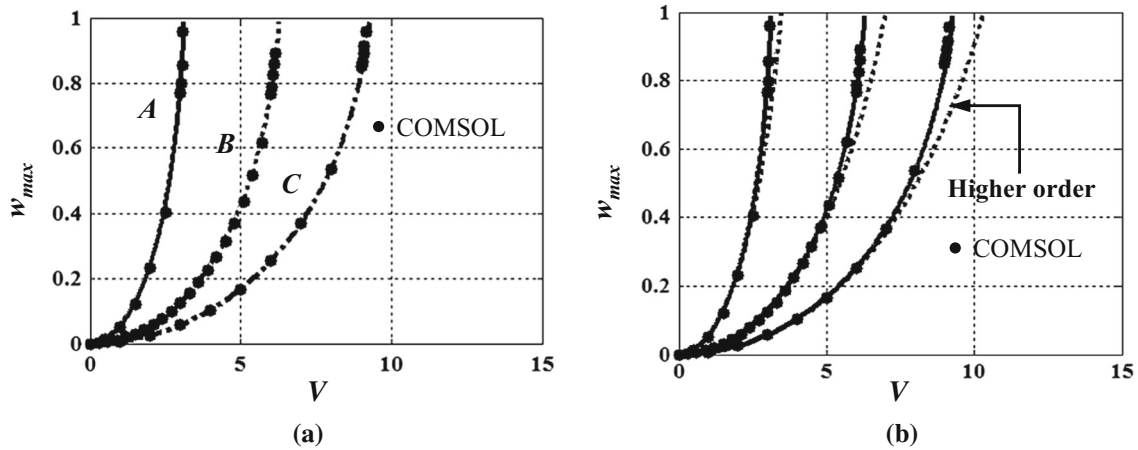


**Fig. 4** **a** Effect of nonlinearity for $a\,\beta = 2.2\text{e}^{-5}$, $b\,\beta = 4.4\text{e}^{-5}$, and $c\,\beta = 6.6\text{e}^{-5}$. **b** Effect of higher-order nonlinearity for $a\,\beta = 2.2\text{e}^{-5}$, $b\,\beta = 4.4\text{e}^{-5}$, and $c\,\beta = 6.6\text{e}^{-5}$

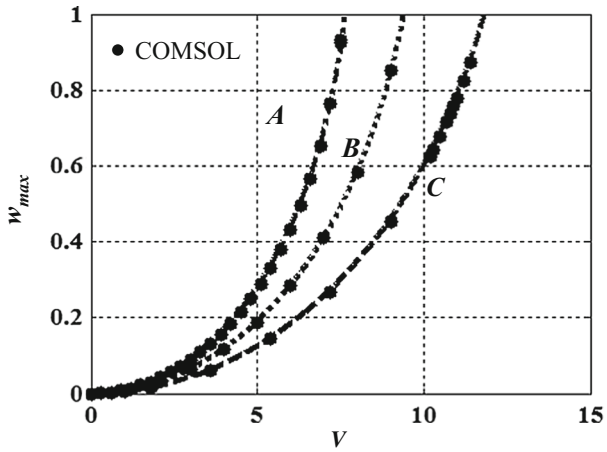


**Fig. 5** Effect of electrode length on maximum deflection ($w_{L_b+L_p}$) of plate end for $a\,\overline{L}_1 = 0.2, \overline{L}_2 = 0.9$, $b\,\overline{L}_1 = 0.2, \overline{L}_2 = 0.8$, and $c\,\overline{L}_1 = 0.2, \overline{L}_2 = 0.7$

critical value called as pull-in voltage. At this critical value, at a further increase in applied voltage, the system approaches a state of unstable via static bifurcation.

The electrostatic microsystem with larger gap ratio experiences a pull-in occurrence at higher voltage, and as a result, the system becomes statically unstable at a higher applied voltage. However, the gap ratio has here been adjusted by changing the size of the microbeam, while the air-gap thickness remains the same. Therefore, the small-scale size movable electrode introduces a higher gap ratio required to have high potential difference to become statically unstable and may be collapsed onto the ground under a certain critical voltage. Hence, it is noteworthy that the small-size electrostatically actuated switch performs satisfactorily in a relatively large operating voltage without pull-in occurrence. Furthermore, it has been observed that the pull-in instability which leads an unexpected collapse onto the ground electrode via bifurcation can easily be controlled by introducing the higher-order structural nonlinearity as observed in Fig. 4b. Also, results obtained using 3D modeling software (represented by solid circles) have been used to examine the correctness of the numerically estimated results, and they have been found to be in very good agreement.

The result of varying the electrode length on the pull-in behavior has been illustrated in Fig. 5. With an increase in electrode length (i.e., $\overline{L}_2 - \overline{L}_1$), the pull-in voltage decreases as the resultant electrostatic force surplaces the restoring force with increase in electrode length. Hence, the pull-in voltage takes place at a lower voltage for increasing the electrode length. It is also noteworthy that higher-order deformation leads to a smaller electrostatic force and builds pull-in occurrence at a higher actuation voltage shown in Fig. 6. Hence, it is therefore important to make a note that the loss of structural stability may take place at a moderately

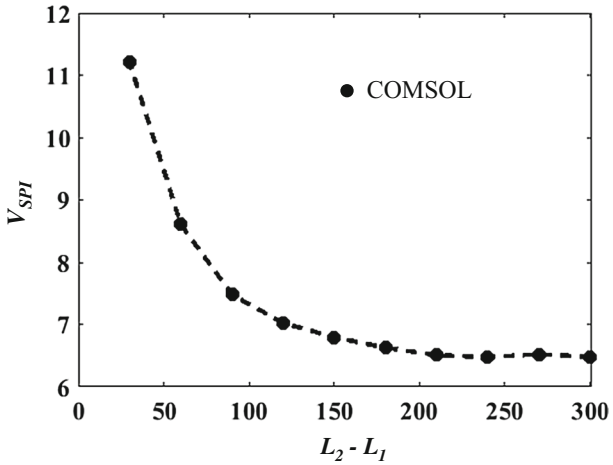


**Fig. 6** Effect of electrode length on pull-in voltage for plate length equal to 45 μm and $L_1 = 0.0$, $\overline{L}_2 = 1.0$

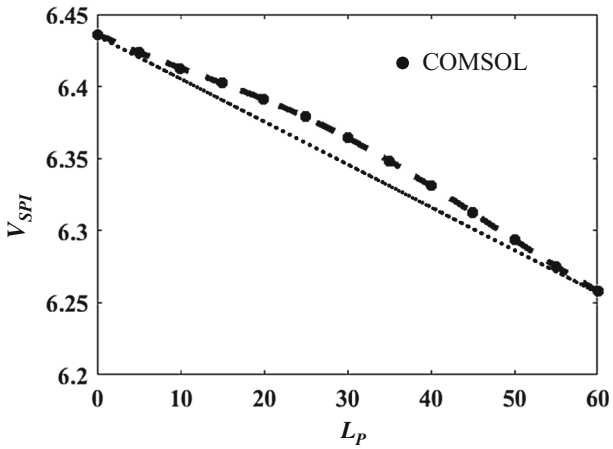


**Fig. 7** Effect of plate length on pull-in voltage for electrode length 300 μm and $L_1 = 0.0$, $\overline{L}_2 = 1.0$

higher voltage when a higher-order correction factor of electrostatic force is included into the dynamic model. Figure 7 demonstrates the effect of plate length on the static pull-in voltage. With increase in electrode length, the pull-in voltage decreases as the effective area moment of inertia increases with an increase in plate length. The pull-in voltage varies almost linearly with the electrode length as represented by the dotted line. A useful understanding of the development of pull-in voltage in dynamic condition via possible bifurcation under linear viscous and squeeze film damping domains is given in the following Subsection.

## 4.2 Dynamic analysis

For determining the static pull-in voltage, the transient part of the applied voltage is neglected by assuming the fact that the rate of applied voltage is negligible. However, to accurately understand the benefits and limitation of the electrostatically actuated device, it is improper only to estimate the static pull-in voltage when a bias alternative voltage source exists. Hence, there is a need to calculate the pull-in voltage called as dynamic pull-in voltage, considering the dynamics of the microbeam instead of static state only. Besides the components which accumulate the strain energy for elastic deformation, inertia and dissipative elements play an influential role in estimating the pull-in voltage in a dynamic condition. Here, the dynamic pull-in behavior has been depicted and investigated for different conditions, i.e., pull-in conditions for the system with and without linear viscous and squeeze film damping. The direct simulation using the well-known Runge–Kutta method has been performed to numerically solve the reduced order governing Eq. (8) in calculating the full-order dynamic pull-in voltages. In this process, dynamic pull-in voltage has been illustrated in the phase portrait, i.e., in the plane of $w \propto \dot{w}$ for

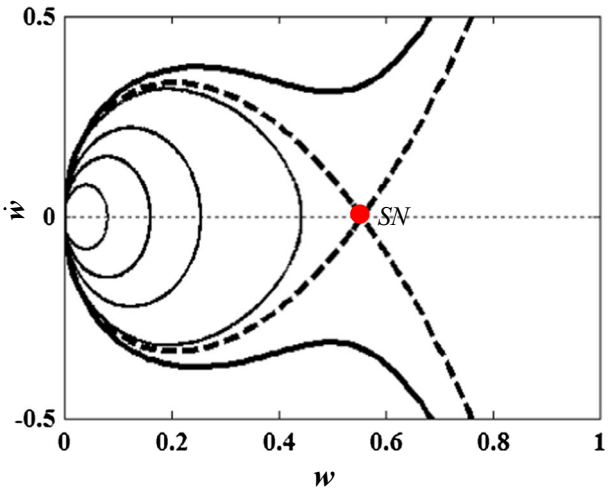


**Fig. 8** Dynamic pull-in voltage of undamped system for electrode length 45 μm and $L_1 = 0.0$, $\overline{L}_2 = 1.0$, and $\beta = 4.4\text{e}^{-5}$

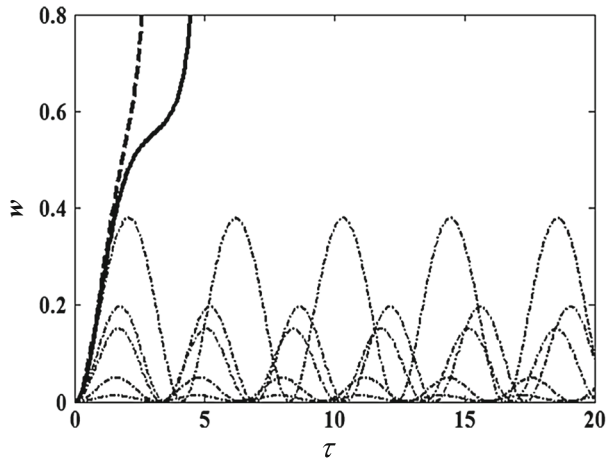


**Fig. 9** Time history of the undamped system for electrode length 45 $\mu m$ and $L_1 = 0.0$, $\overline{L}_2 = 1.0$, and $\beta = 4.4\text{e}^{-5}$

every applied voltage within the range $0 < V \leq V_{static}$, knowing the fact that the dynamic pull-in voltage is lower than that of the static counterpart. The dynamic pull-in voltage has been diagrammed for various control parameters such as plate length, electrode length, order of nonlinearity, air-gap thickness, and squeeze film damping on dynamic pull-in voltage. The trajectories have been drawn for the voltage starting from zero to the voltage until it leads to an intersection of the orbits with the origin.

Figure 8 depicts the pull-in dynamics for an undamped system while keeping the electrode length equal to the length of the microbeam. The dynamic pull-in voltage has been apprehended by the monoclinic orbits passing through the saddle node or degenerate singularity point. The system becomes dynamically unstable when a slight increase in voltage at the critical voltage $V_{\text{DPI}} = 4.262$ happens, and it was found that the dynamic pull-in voltage is well below the static pull-in voltage $V_{\text{SPI}}$, i.e., nearly 75 % of $V_{\text{SPI}}$. For applied voltage $V < V_{\text{DPI}}$, the system is dynamically stable and exhibits closed periodic orbits with steady response amplitude lower than the dynamic pull-in deflection. Hence, a periodic solution developed from an initial guess for a certain voltage always builds a closed trajectory which represents a neutrally stable center as time approaches infinity. Hence, for every applied voltage $V < V_{\text{DPI}}$, the system shows an isolated stable closed trajectory.

On the contrary, the voltage for dynamic instability is well below that of the static counterpart, and hence, it is advisable to keep the actuation voltage $V < 4.262$ to avoid uninterrupted performance of the device due to pull-in phenomenon. The time history of the dynamic deflection is illustrated in Fig. 9, and it has been observed that the pull-in deflection occurs at 0.56 for the undamped system. Similar to the pull-in voltage, the dynamic

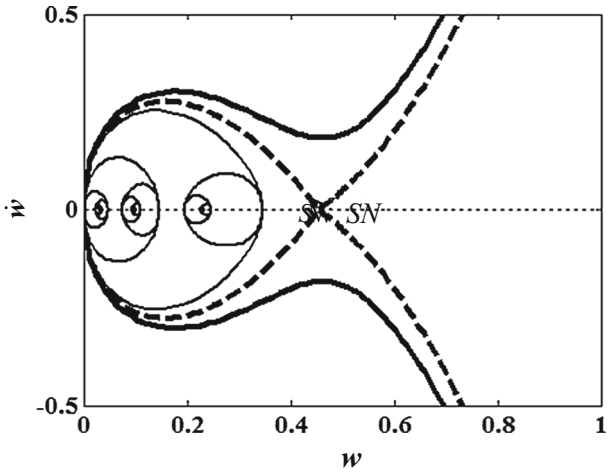


**Fig. 10** Dynamic pull-in voltage of the under-damped system for plate length 45, $\beta = 4.4\text{e}^{-5}$ and $c = 0.91$ N s/m$^2$

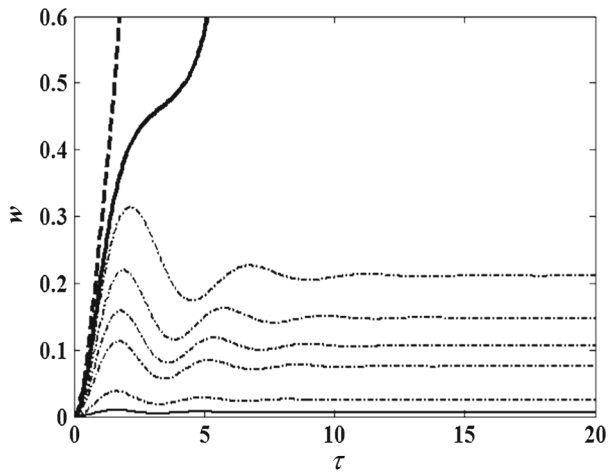


**Fig. 11** Time history of the under-damped system for electrode length 45, $\beta = 4.4\text{e}^{-5}$ and $c = 0.91$ N s/m$^2$

deflection has been found to be a smaller value than the static tip deflection. The pull-in voltages estimated via time history and phase portrait have been quantitatively compared and found to be in good agreement. Since the fundamental natural frequency of the device decreases with an increase in actuation voltage, the time period of the response hence increases with an increase in voltage. An unstable divergent motion encounters from a periodic motion at a voltage equal to $V_{\text{DPI}} = 4.26$, and as a result, the beam may catastrophically fail onto the fixed electrode. However, the problem of pull-in instability can be attenuated by introducing the damping mechanisms in the form of viscous and squeeze film damping.

Here, the dynamic pull-in voltage has been investigated for the system with damping for $L_1 = 0.0$, $\overline{L}_2 = 1.0$. The dynamic pull-in voltage is found to be 4.48 for the system with damping factor ($\zeta$) equal to 0.465, while the critical value of dynamic pull-in voltage for the system with squeeze film is observed to be 4.54 as shown in Figs. 10 and 12. Hence, the pull-in voltage increases with the presence of air-damping mechanism confined in the air gap between the electrodes. Also, pull-in performance materializes at a lower deflection as compared to the deflection for the undamped system. Hence, the it has been found that the squeeze film damping makes the system more stable dynamically (Figs. 11, 12).

The time history of the dynamic tip deflection for the under-damped system has been shown in Fig. 11, while the time history of dynamic tip deflection for the system with squeeze film has been depicted in Fig. 13. From these illustrations, it is clear that the amplitude of the responses decays exponentially for the system with viscous damping, whereas squeeze film damping renders faster decaying of amplitude which results in

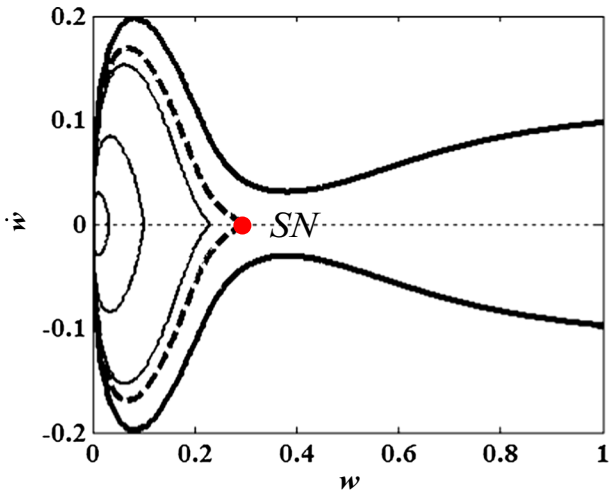


**Fig. 12** Dynamic pull-in voltage of under-damped system with squeeze film for electrode length 45 μm, $\overline{L}_2 - \overline{L}_1 = 1.0$, $\beta = 4.4\text{e}^{-5}$, and $\mu = 1.86 \times 10^{-5}$ N s/m$^2$

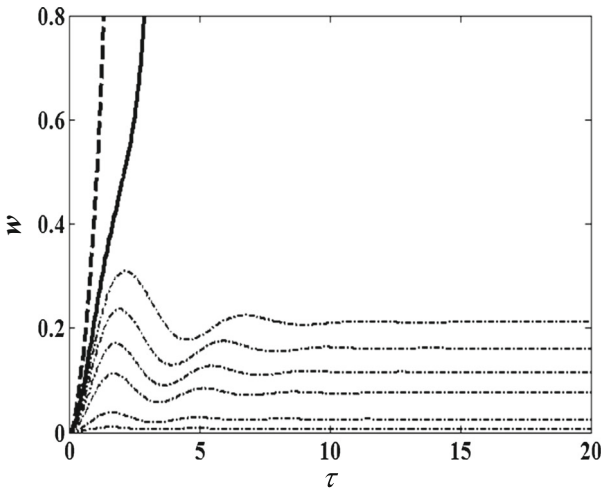


**Fig. 13** Time history of under-damped system with squeeze film for electrode length 45 μm, $\beta = 4.4\text{e}^{-5}$, $\overline{L}_2 - \overline{L}_1 = 1.0$ and $\mu = 1.86 \times 10^{-5}$ N s/m$^2$

a lower settling time. However, a clear picture of the variation of pull-in stability for all three cases has been illustrated in Fig. 14.

Figure 15 depicts the effect of changing rigid plate length on the dynamic pull-in voltage for the undamped system with $\beta$ equal to $4.4\times10^{-5}$, $L_1 = 0.0$, and $\overline{L}_2 = 1.0$. It is noteworthy that with the increase in plate length, the pull-in voltage decreases while the dynamic tip deflection increases with increase in plate length. Since the inertia effect, i.e., a destabilizing factor of the microsystem, dominates with the increase in plate size, the dynamic pull-in instability occurs at a lower voltage. Furthermore, the settling time of the responses increases with increases in plate length since the natural frequency decreases with the increase in overall mass of the beam-plate microsystem. Hence, because of the presence of the plate, the inertia force adds up with the electrostatic force, and the effective destabilizing factor surpluses the overall restoring force. Therefore, pull-in instability encounters at a low actuation voltage.

Figure 16 demonstrates the influence of geometric flexibility $\beta$ on the dynamic pull-in voltage for the undamped system. Here, the factor $\beta$ has been obtained by changing the length of the microbeam while keeping the air-gap constant. Similar to the static analysis, here also the system becomes dynamically unstable at a higher applied voltage for relatively high structural nonlinearity as $\beta = 2.2 \times 10^{-4}$. For example, the dynamic pull-in voltage was found to be 15.956 for $\beta$ equal to $2.2 \times 10^{-4}$, while the dynamic pull-in voltage

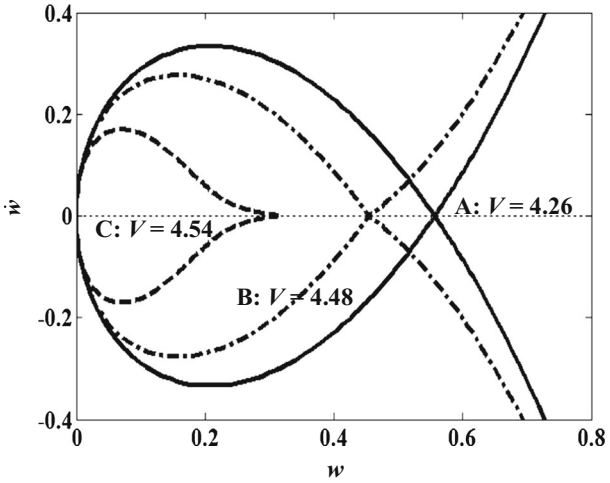


**Fig. 14** Dynamic pull-in voltage: *A* undamped system *B* damped system *C* system with squeeze film effect

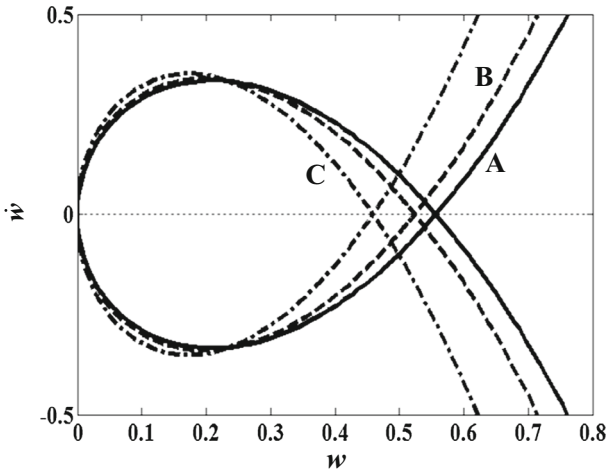


**Fig. 15** Influence of rigid plate length on dynamic pull-in voltage for: *A* $L_p = 60\,\mu m$, *B* $L_p = 45\,\mu m$, and *C* $L_p = 30\,\mu m$

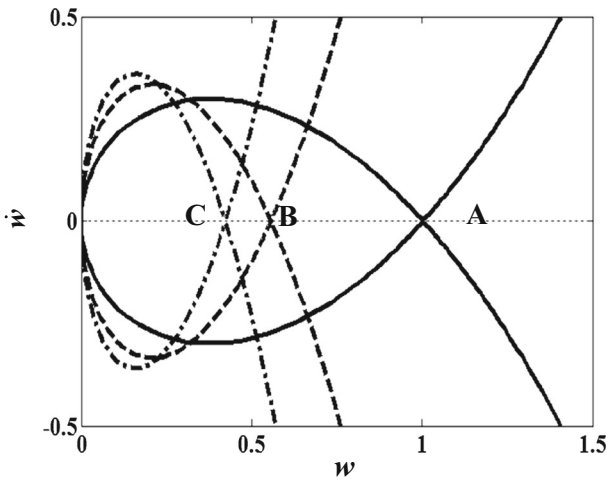


**Fig. 16** Influence of gap–length ratio ($d_0/L_b$) on dynamic pull-in voltage for $L_p$ equal to 45 μm: *A* $\beta = 4.4\text{e}^{-4}$, *B* $\beta = 4.4\text{e}^{-5}$, and *C* $\beta = 4.4\text{e}^{-6}$

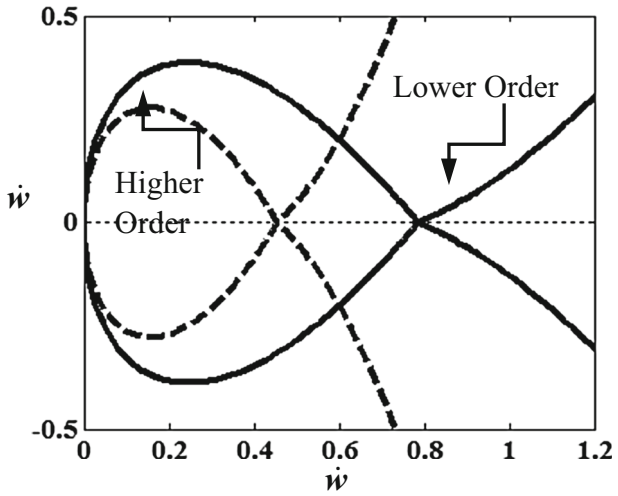


**Fig. 17** Influence of higher-order electrostatic force on dynamic pull-in voltage for plate length 45 μm, $a\,\overline{L}_1 = 0$, $\overline{L}_2 = 1.0$ and $\beta = 4.4\text{e}^{-5}$

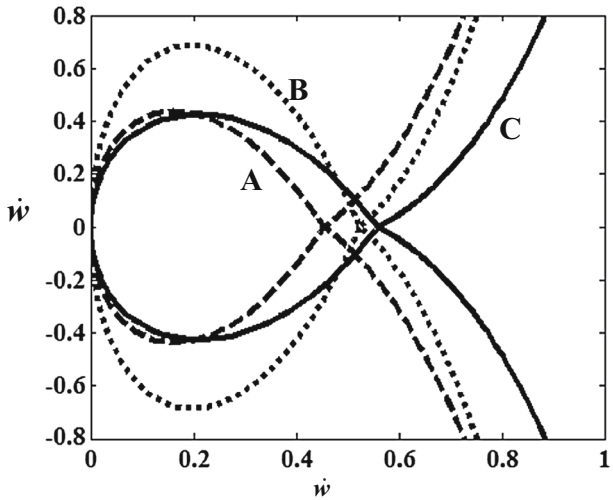


**Fig. 18** Influence of electrode length on dynamic pull-in voltage for plate length 45 μm and $\beta = 4.4\text{e}^{-5}$, for $a\overline{L}_1 = 0$, $\overline{L}_2 = 1.0$, $b\overline{L}_1 = 0.1$, $\overline{L}_2 = 0.9$, and $c\overline{L}_1 = 0.2$, $\overline{L}_2 = 0.8$.

was observed to be 1.446 for $\beta$ equal to $6.6 \times 10^{-6}$. Hence, it is worthy to note that a reduction in size of the device establishes more structural stability as dynamic pull-in occurs at high actuation voltage. Operating the system with high air-gap length ($d$) is safe under relatively high voltage input. Simultaneously, to develop an efficient and effective electrical switch, the designer should always prefer to keep the air-gap length ratio at a lower order which results pull-in instable at low actuation voltage for operating within ON and OFF conditions.

Figure 17 provides how the dynamic pull-in voltage gets influenced by the terms of order $(1-w)^{-2}$. Here, the influence of both higher order comprising the first seven terms, i.e., $1 + 2w + 3w^2 + \cdots 7w^6$, and lower order consisting of the first two terms, i.e., $1 + 2w$, on the dynamic pull-in voltage has been investigated. It has been observed that electrostatic pressure developed by considering the higher-order terms undergoes the dynamic pull-in voltage at lower applied voltage as the effective electrostatic force exceeds the restoring force at low actuation voltage, and it is found to be $3.86 < V_{\text{DPI}} = 4.26$.

The influence of electrode length on estimation of pull-in voltage has been investigated in Fig. 18. With a decrease in electrode length, the pull-in instability occurs at a higher value. It has been observed that for the electrode length equal to 0.9 times the length of the microbeam, the dynamic pull-in voltage occurs at a value equal to 5.2. A similar trend has been observed when the electrode length is 0.8 times the length of the microbeam, and, in this case, the pull-in voltage has come out to be 6.78. Therefore, the effective electrostatic force relies on the effective length of the electrode as well as the location of the electrode. Also, the distribution

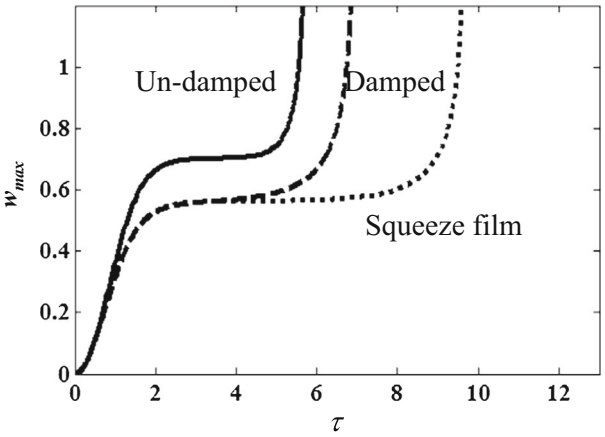


**Fig. 19** Time history at pull-in voltage for undamped, damped and system with squeeze film for electrode length 45 μm keeping the other parameters constant

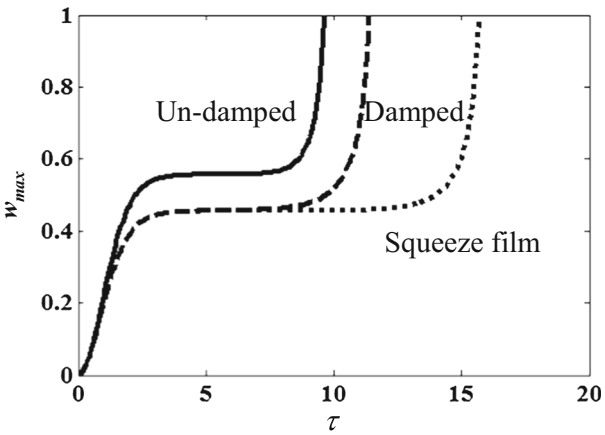


**Fig. 20** Time history at pull-in voltage for undamped, damped and system with squeeze film for electrode length 60 μm keeping the other parameters constant

of the electrostatic pressure is significant when the electrode moves toward the end point of the beam. The induced electrostatic force is found to be maximum when the ground electrode is positioned closest to the end of the beam since $(1 - w)$ becomes minimum at $L_b$.

Figures 19 and 20 demonstrate the time history obtained by integrating the equation of motion (8) at pull-in voltage where the system loses its stability due to dynamic pull-in. A slight increase in voltage at $V = V_{\text{DPI}}$, a periodic motion, exhibits a divergent motion, which abruptly collapses the beam onto the electrode. The divergent motion has been observed at dynamic pull-in voltage same as that estimated from the trajectories in the phase plane for various situations. The periodic response has been seen before approaching into dynamic pull-in instability for an undamped system. For a certain value of applied bias voltage, an aperiodic solution may observe due to the fact of including an air-damping mechanism for small air-gap thickness as shown in Fig. 20. It has been noted that the transient part of the time history has been reduced by adding a damping parameter as the response amplitude gets exponentially decayed. Moreover, it has been revealed that a desired performance can be established from the devices via introducing the dissipation (Fig. 21).

## 5 Conclusions

A cantilever-based microbeam coupled with a rigid plate has been used to mathematically model an electrostatically actuated microswitch. To obtain a more accurate estimation of pull-in instability in static and dynamic conditions, a comprehensive mathematical model has been developed accounting for structural nonlinearity and resultant higher-order electrostatic pressure and nonlinear air film damping. The effect of various design parameters on the estimation of static and dynamic pull-in behavior has been studied. The structural stability

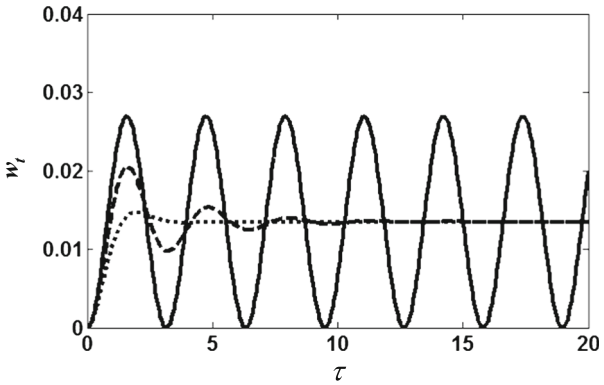


**Fig. 21** Time history of the system *a* undamped *b* under-damped *c* under-damped with squeeze film effect for the electrode length is 45 μm

of the switch has been critically assessed by the realization of pull-in voltage when the design parameter varies. However, the following practical implication of microswitch by the realization of its behavior under the varied bias voltage is:

(i) Dynamic pull-in voltage is observed to be lower than that of static pull-in voltage. The dynamic pull-in instability takes place at a lower applied voltage when the higher-order terms of electrostatic force are employed.
(ii) A high scaling factor of geometric and inertial nonlinearities ($\beta$) makes the microsystem statically and dynamically stable. Unfortunately, a small scaling factor makes the microsystem more sensitive with respect to pull-in instability for low applied voltage.
(iii) With the increase in electrode length, the pull-in voltage gets decreased while it becomes higher for considering viscous and squeeze film damping. It is worthy to note that with the increase in plate length, the pull-in voltage decreases while pull-in deflection occurs at a higher value with the increase in plate length.
(iv) Structural stability improves the combined effect of squeeze film and linear viscous damping. Pull-in behavior occurs at lower tip deflection compared to the static pull-in deflection due to the additional effect of inertia.
(v) The microsystem requires high voltage to become dynamically unstable for relatively high structural nonlinearities.
(vi) A closed trajectory of periodic response has been observed for the voltage less than the critical value at which the system undergoes pull-in instability, whereas aperiodic response may be observed for the system with damping mechanism.
(vii) The results from this research enable a significant understanding of pull-in operation under the variation of several control parameters. These results are useful to an operator while dealing with the operation of an electrostatically actuated microswitch.

**Acknowledgments** Authors thank Professor Ambesh Dixit, Department of Physics, Indian Institute of Technology Jodhpur, for his support in providing COMSOL Multi-physics software.

## References

1. Rebeiz, G.M.: RF MEMS Theory, Design and Applications. Wiley, New Jersey (2003)
2. Vardan, V.K., Vinoy, K.J., Jose, K.A.: RF MEMS and Applications. Wiley, West Sussex (2003)
3. Adams, S.G., Bertsch, F.M., Shaw, K.A., Macdonald, N.C.: Independent tuning of linear and nonlinear stiffness coefficients. J. Microelectromech. Syst. **71**, 72–80 (1998)
4. Kim, S., Mani, S., Boyd, J.G.: Modelling of mechanical behavior of micro-cantilever due to intrinsic strain during deposition. J. Mech. Sci. Technol. **20**, 1646–1652 (2006)
5. Senthil Kumar, P. K., Elavarasi, R., Braineard Eladi, P., Gopikrishnan, M.: Pull-in voltage study of various structured cantilever and fixed-fixed beam models using COMSOL multiphysics. Indian J. Sci. Technol. **8**, 1–9 (2015)
6. Lee, L.S., Howell, S.W., Rahman, A., Reifenberger, R.: Nonlinear dynamics of micro cantilevers in tapping mode atomic force microscopy: a comparison between theory and experiment. Phys. Rev. B **66**, 115409-10–115410 (2002)

7. Lee, J.W.: Analysis of fluid-structure interaction for predicting resonant frequencies and quality factors of a micro-cantilever on squeeze film. J. Mech. Sci. Technol. **25**, 5–13 (2011)
8. Wang, P.K.C.: Bifurcation of equilibria in micromachined elastic structures with electrostatic actuation. Int. J. Bifurc. Chaos **11**, 469–482 (2011)
9. Elata, D., Nemirovsky, Y.: An efficient DIPIE algorithm for CAD of electrostatically actuated MEMS devices. J. Microelectromech. Syst. **11**, 612–620 (2002)
10. Luo, A. C. J., Wang, F.Y.: Chaotic motion in a micro-electro mechanical system with non-linearity from capacitors. Commun. Nonlinear Sci. Numer. Simul. **7**, 31–49 (2002)
11. Gabbay, L.D., Mehner, J.E., Senturia, S.D.: Computer aided generation of nonlinear reduced order macromodels-II: stress-stiffenedcase. J. Microelectromech. Syst. **9**, 270–278 (2000)
12. Ramezani, A., Alasty, A., Akbari, J.: Closed-form solutions of the pull-in instability in nano-cantilevers under electrostatic and intermolecular surface forces. Int. J. Solids Struct. **44**, 4925–4941 (2007)
13. Nayfeh, M., Younis, M.I., Abdel-Rahman, E.M.: Dynamic pull-in phenomenon in MEMS resonators. Nonlinear Dyn. **48**, 153–163 (2007)
14. Abdel-Rahman, E.M., Younis, I., Nayfeh, A.H.: Characterization of mechanical behavior of an electrically actuated microbeam. J. Micromech. Microeng. **12**, 759–766 (2002)
15. Haluzan, D.T., Klymyshyn, D.M., Achenbach, S., Borner, M.: Reducing pull-in voltage by adjusting gap shape in electrostatically actuated cantilever and fixed-fixed beams. Micromachines **1**, 68–81 (2010)
16. Dominicus, J.I., Talimass, J., Harrie, A.C.: Static and dynamic aspects of an air gap capacitor. Sens. Actuators A: Phys. **35**, 121–128 (1992)
17. Mojahedi, M., Moghimi, M.Z., Ahmadian, M.T.: Static pull-in analysis of electrostatically actuated microbeams using homotopy perturbation method. Appl. Mathem. Model. **34**, 1032–1041 (2010)
18. Busta, H., Amantea, H., Furst, D., Chen, J.M., Turowski, M., Mueller, C.: A MEMS shield structure for controlling pull-in forces and obtaining increased pull-in voltages. J. Micromech. Microelectron. **11**, 720–725 (2001)
19. Zhang, S., Meng, G.: Nonlinear dynamical system of micro-cantilever under combined parametric and forcing excitations in MEMS. 30th Annual Conference of IEEE 2 pp. 1571–1576. (2004)
20. Liu, S., Davidson, A., Lin, Q.: Simulating nonlinear dynamics and chaos in a MEMS cantilever using Poincaré mapping *IEEE*: Transducers-12th International Conference on Solid State Sensors, Actuators and Microsystems, Boston pp. 1092–1095. (2003)
21. Gang, Li, Aluru, N.R.: Linear, nonlinear and mixed-regime analysis of electrostatic MEMS. Sens. Actuators A: Phys. **91**, 278–291 (2001)
22. Ashby, M.F.: Multi-objective optimization in material design and selection. Acta Mater. **48**, 359–369 (2000)
23. Gabbay, L.D., Mehner, J.E., Senturia, S.D.: Computer-aided generation of nonlinear reduced-order dynamic macro models—I: non-stress-stiffened case. J. Microelectromech. Syst. **92**, 62–69 (2000)
24. Furlani, E.P.: Theory and simulation of viscous damped reflection phase gratings. J. Phys. D: Appl. Phys. **32**, 412–418 (1998)
25. Krylov, S., Mainom, R.: Pull-in dynamics of an elastic beam actuated by continuously distributed electrostatic force. J. Vib. Acoust. **126**, 332–342 (2004)
26. Chao, P.C.P., Chiu, C.W., Liu, T.H.: DC dynamic pull-in predictions for a generalized clamped-clamped micro-beam based on a continuous model and bifurcation analysis. J. Micromech. Microelectron. **18**, 115008 (2008)
27. Chaterjee, S., Pohit, G.: A large deflection model for the pull-in analysis of electrostatically actuated micro-cantilever beams. J. Sound Vib. **322**, 969–986 (2009)
28. Pratiher, B.: Stability and bifurcation of an electrostatically controlled highly deformable micro-cantilever based resonator. Nonlinear Dyn. **78**, 1781–1800 (2014)
29. Kivi, A.R., Azizi, A., Marzbanrad, J.: Investigation of static and dynamic pull-in instability in a FGP micro-beam. Sens. Imaging **16**, 2 (2015)
30. Jia, X., Ke, L., Feng, C., Yang, J., Kitipornchai, S.: Size effect on the free vibration of geometrically nonlinear functionally graded micro-beams under electrical actuation and temperature change. Compos. Struct. **133**, 1137–1148 (2015)
31. Jiao, Xl, Yang, J., Kitipornchai, S.: Pull-in instability of geometrically nonlinear micro-switches under electrostatic and Casimir forces. Acta Mech. **218**, 161–174 (2011)
32. Moeenfard, H., Darvishian, A., Ahmadian, M.T.: A coupled bending-torsion model for electrostatically actuated torsional nano/micro-actuators with considering influence of van der Waals force. Acta Mech. **224**, 1791–1800 (2013)
33. Ramezani, A., Alasty, A.: Combined action of Casimir and electrostatic forces on nanocantilever arrays. Acta Mech. **212**, 305–317 (2010)
34. Wang, C., Guo, W., Feng, Q.: Deflection and stability of membrane structures under electrostatic and Casimir forces in microelectromechanical systems. Acta Mech. **180**, 49–60 (2005)
35. Duan, J., Li, Z., Liu, J.: Pull-in instability analyses for NEMS actuators with quartic shape approximation. Appl. Math. Mech. **36**, 1–12 (2015)
36. Pratap, R., Mohite, S., Panday, A.K.: Squeeze-film effects in MEMS devices, invited paper. J. Indian Inst. Sci. **87**, 75–94 (2007)
37. Pandey, A.K., Pratap, R.: Studies in nonlinear effects of squeeze film damping in MEMS structures. Int. J. Comput. Eng. Sci. **4**, 477–480 (2003)
38. Mcgarthy, B., Adams, G.G., Mcgruer, N.E., Potter, D.: A dynamic model including contact bounce of an electrostatically actuated microswitch. J. Micro-electromech. Syst. **13**, 276–283 (2002)
39. Rocha, L.A., Mol, L., Cretu, E., Wolffenbutte, R.F.: Experimental verification of squeezed-film damping models for MEMS. ASME: Int. Mech. Eng. Congr. Expos. **6**, 89–93 (2006)
40. Veijola, T., Raback, P.: Methods for solving gas damping problems in perforated microstructures using a 2d finite-element solver. Sensors **7**, 1069–1090 (2007)